ISSN 0869-5911, Petrology, 2022, Vol. 30, No. 6, pp. 591–609. © Pleiades Publishing, Ltd., 2022.
Russian Text © The Author(s), 2022, published in Petrologiya, 2022, Vol. 30, No. 6, pp. 623–643.

The Great Dyke of the Kola Peninsula as a Marker of an Archean Cratonization in the Northern Fennoscandian Shield

A. V. Stepanova[a, *], A. V. Samsonov[b], E. B. Salnikova[c], S. V. Egorova[d], Yu. O. Larionova[b], A. A. Arzamastsev[c], A. N. Larionov[d], M. A. Sukhanova[c], and R. V. Veselovskiy[e, f]

[a] *Institute of Geology, Karelian Research Centre, RAS, Petrozavodsk, Russian Federation*
[b] *Institute of Geology of Ore Deposits, Petrography, Mineralogy and Geochemistry RAS, Moscow, Russian Federation*
[c] *Institute of Precambrian Geology and Geochronology, RAS, Saint-Petersburg, Russian Federation*
[d] *Centre for Isotopic Research, Russian Geological Research Institute, Saint-Petersburg, Russian Federation*
[e] *Institute of Physics of the Earth, RAS, Moscow, Russian Federation*
[f] *Geological Faculty, Lomonosov Moscow State University, Moscow, Russian Federation*
**e-mail: stepanov@krc.karelia.ru*

Received May 19, 2022; revised June 11, 2022; accepted June 18, 2022

Abstract—The results of geochronological and petrological studies of the largest mafic dyke in the northern part of the Fennoscandian Shield, called the Great Dyke of the Kola Peninsula (GDK), are presented. According to U-Pb D-TIMS baddeleyite dating, the GDK crystallization age is 2680 ± 6 Ma. The age of host granites is 2.75–2.72 Ga (U-Pb, zircon, SHRIMP-II). The dyke has a simple internal structure with no signs of multistage melt injection. It comprises equigranular and plagioclase-porphyritic dolerites and gabbro that are amphibolitized to varying degrees. All rocks are low-Mg (Mg# less than 0.37) with low concentrations of Cr and Ni, and were derived through differentiation of more primitive melts. The analysis of geochemical and Sr-Nd isotopic data suggests that GDK melts could be formed by mixing of two types of mantle melts: depleted asthenospheric melt and enriched melt formed via melting of a lithospheric mantle. The weakly fractionated HREE patterns indicate that primary GDK melts originated at shallow (<60 km) depths outside the garnet stability field. The generation and injection of melts of the Neoarchean GDK occurred immediately after large-scale granitic magmatism and main crustal growth event in the Murmansk Craton and marked the cratonization of the continental lithosphere in the northeastern part of the Fennoscandian Shield.

Keywords: Neoarchean, mafic dykes, baddeleyite, U-Pb ID-TIMS

DOI: 10.1134/S086959112206008X

INTRODUCTION

Megadykes that are the large bodies reaching a length over 100 km (Ernst and Bell, 1992) are rare among mafic dykes. They represent large channels of magma transport and give insights into mechanisms of a melt migration during formation of large igneous provinces (LIPs). Mafic dyke swarms and megadykes are formed under extensional settings, and the largest dykes considered to be formed due to melt injection in the pre-existing weakened zones (Pollard, 1987; Hoek, 1994). A few megadykes are known worldwide, and all of them are studied in detail. The most known are the Neoarchean (2575.4 ± 0.7 Ma; Oberthür et al., 2002) Great Dyke of Zimbabwe that is over 550 km long and 11 km thick, the Great Abitibi Dyke (1141 ± 2 Ma) ~ 700 km long in the Superior Province, Canadian Shield (Krogh et al., 1987; Ernst and Bell, 1992), Ahmeyim Great Dyke of Mauritania (2.73 Ga; Tait et al., 2013), and Mesoproterozoic (1629 ± 1 Ma) dyke in West Greenland (Kalsbeek and Taylor, 1986; Halls et al., 2011). The Tertiary (58.4 ± 1.1 Ma) Cleveland Dyke forms an en echelon body 400 km long (Macdonald et al., 1988). In situ differentiation is observed in all these dykes and is best expressed in the Zimbabwe dyke, which is considered by many researchers as a PGE-bearing layered intrusion (Wilson, 1992; Oberthür et al., 2002).

Mafic dykes regarded as a component of feeding system of large igneous provinces (Ernst et al., 2019) record not only timing of rifting and uplift related with mantle plume ascent, but also such processes as back-arc basin extension, orogen collapse, and crustal stabilization, which are not related to the mantle plume activity (Cottin et al., 1998; Ernst, 2014; Klausen, 2020). The wide diversity of tectonic settings in which mafic dykes exist allowed M. Klausen to subdivide large igneous provinces into two types: "breakup" provinces formed during supercontinental fragmentation, and "assembly" provinces that record the amalgamation of supercontinents (Klausen, 2020). Mafic

rocks of these two types of LIPs differ not only in tectonic settings and relations with supercontinent breakup or assembly, but also in mantle sources composition and contribution of lithospheric and plume components (Klausen, 2020).

In the orogenic belts, the post-collisional stage that terminates the orogenic cycle is associated with lithosphere extension and delamination, upwelling of asthenosphere and characterized by a large-scale magmatic activity, metamorphism, and crustal anatexis (Bonin, 2004). In this series, intrusive mafic rocks serve as an important time and genetic markers (Bonin, 2004; Kingsbury et al., 2021; Wang et al., 2022). At the same time, the emplacement of mafic rocks simultaneously with granitoids and granite pegmatites is also typical of Proterozoic anorthosite–rapakivi–granite associations (Shumlyanskyy et al., 2021; Johansson et al., 2022). However, the geodynamic nature of the basaltic melts and their relations with granitoids remain controversial.

In contrast to enriched mafic rocks of high-K or calc-alkaline series, whose tectonic setting and origin in post-orogenic environments are well studied (Song et al., 2015; Xu et al., 2020, and references therein), the genesis of tholeiitic series mafic rocks in post-orogenic environments is problematic, and tectonic position of dyke swarms and origin of melts sequence remain an unresolved. It is relevant whether dyke swarms mark orogenic collapse and termination of the Wilson cycle or record the onset of rifting and start of a new Wilson cycle, and supercontinent fragmentation (Bonin, 2004; Sun et al., 2022).

This work reports first data on the composition, structure, an age of the largest dyke known in the northeastern Fennoscandian shield, the Great Dyke of the Kola Peninsula (GDK). New age, geochemical, and isotopic data on host granitoids and their mafic enclaves are used to evaluate the geodynamic positon of GDK and its place in the evolution of the Murmansk Craton.

REGIONAL GEOLOGY

The Kola part of the Fennoscandian shield comprises Archean and Paleoproterozoic rocks and is subdivided into the Kola and Belomorian tectonic provinces and the Murmansk Craton (Balagansky et al., 2006; Hölttä et al., 2008) (Fig. 1a). The rocks of the Kola and Belomorian provinces adjacent to the Paleoproterozoic Lapland–Kola collisional orogen, experienced strong reworking during 1.93–1.87 Ga orogeny (Balagansky et al., 1998; Daly et al., 2001, 2006). The Murmansk Craton is distinguished as a narrow band in the northern part of the Fennoscandian shield along the Barents Sea coast. It avoided a Paleoproterozoic tectono-metamorphic reworking because of distant position from the Lapland–Kola orogen (Fig. 1a). The boundary of the Kola Province and the Murmansk Craton is a narrow linear tectonic zone marked by the rocks of the Kolmozero–Voron'ya greenstone belt (*Rannii dokembrii* ..., 2005; Kozlov et al., 2006).

According to geological mapping results (an overview in Kozlov et al., 2006), the Murmansk Craton consists mainly of granitoids. The most abundant tonalite–trondhjemite–granodiorite series orthogneisses and granitoids contain scarce metamafic enclaves, which are considered as remnants of reworked greenstone belts. Subalkaline mafic rocks, diorites, and granodiorites compose small separate massifs in different parts of the Murmansk Craton. The mild-alkaline granodiorites and leucogranites are widespread in the western part of the craton, in the Teriberka area, and occur as small massifs at the other territory of the Murmansk Craton (Kozlov et al., 2006). Geochronological data on enderbites of the Kanentjavr massif (2772 ± 7 Ma) and on amphibolites, gneisses, enderbites, diorites, trondhjemites, and granites in the Iokanga area (2.72–2.78 Ma) indicate that the main crustal growth episodes in the Murmansk Craton occurred within 2.7–2.8 Ga (Kozlov et al., 2006). According to Sm-Nd isotopic data, gneisses and granitoids from different parts of the Murmansk Craton have model ages $T_{Nd}(DM)$ from 2.73 to 3.04 Ga (Timmerman and Daly, 1995; Kozlov et al., 2006; Pozhilenko et al., 2018), indicating a relatively short crustal residence of this Meso-Neoarchean continental block.

The Archean granitoids of the Murmansk Craton are intersected by dolerite and olivine gabbro dykes of mainly meridional and northwestern (340°–355°) strike. The U-Pb baddeleyite and zircon age data define at least five groups of mafic dykes and sills with age ca. 2.68, 2.50, 1.98, 1.86, and 0.38 Ga in the Murmansk Craton (Arzamastsev et al., 2009; Fedotov et al., 2012; Stepanova et al., 2018; Veselovskiy et al., 2019).

The Zarubikha dyke (*Geologiya USSR. Murmanskaya oblast*, 1958; Fedotov et al., 2012, and references therein) called by V.S. Kulikov the Great Dyke of the Kola Peninsula (2016, personal communication) occupies a special place among mafic dykes of the Murmansk Craton. The Great Dyke of the Kola Peninsula (GDK) is located in the western part of the Barents Sea coast of the Kola Peninsula. It forms NE-trending (10°–20°) en-echelon body traced from the Medvezh'ya Bay of the Barents Sea through Lake Uelkjavr along the Zarubikha River to Lake Kanentjavr (Fig. 1b). The body is over 50 km long and 150–700 m thick, reaching maximum thickness on the southern coast of Lake Uelkjavr (Fig. 1). A series of late NW-trending faults formed an en-echelon morphology of the body (Fig. 1b). We studied the northernmost segment of the dyke exposed in the Medvezh'ya Bay area, Barents Sea (Fig. 1c).

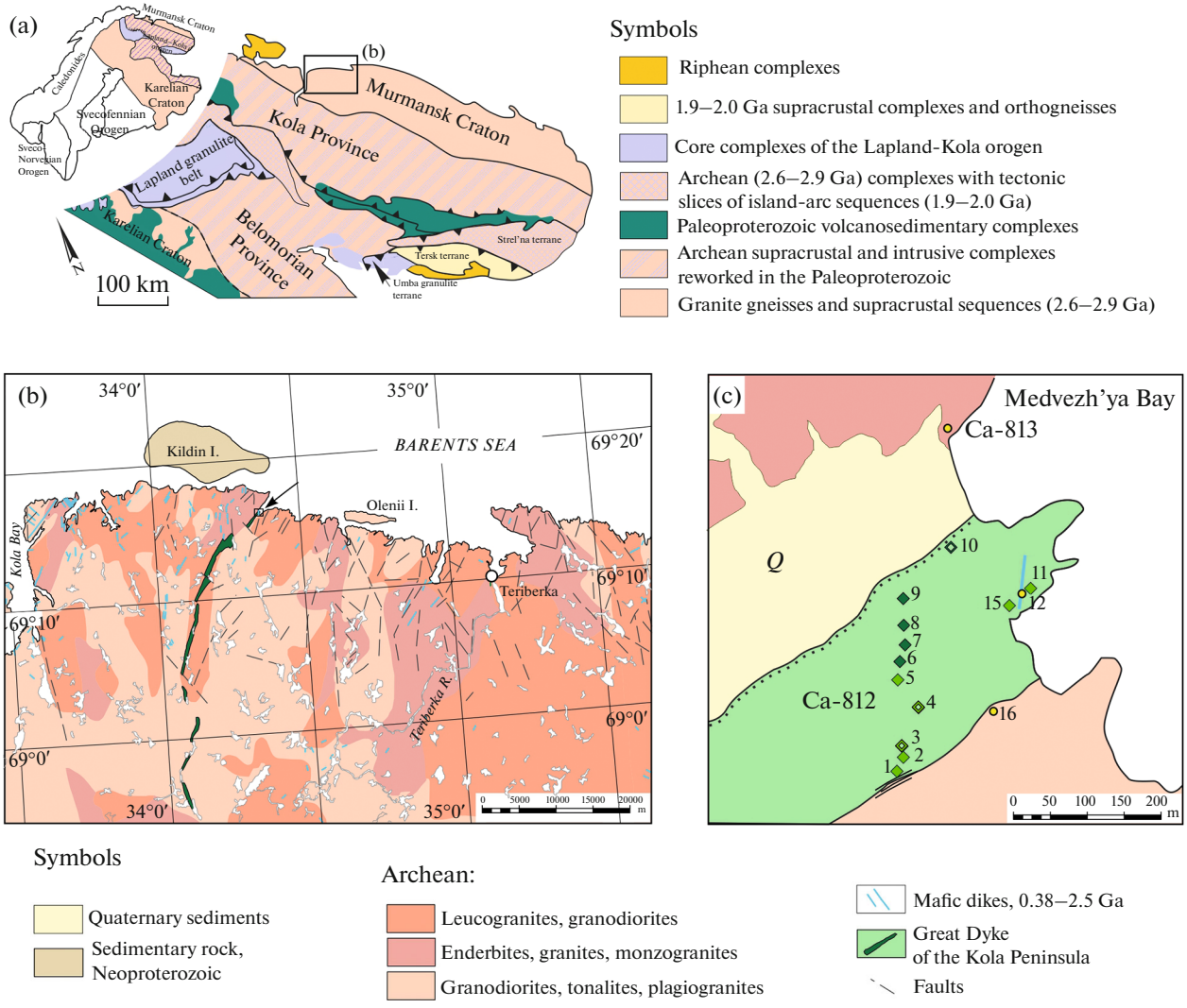

Fig. 1. Geological position of GDK. (a) Tectonic scheme of the northeastern Fennoscandian shield, modified after (Balagansky et al., 2006). Inset shows a scheme of tectonic zoning of Fennoscandia (Hölttä et al., 2008; Bogdanova et al., 2016). (b) Geological scheme of the northwestern part of the Murmansk Craton. Compiled using State Geological Map on a scale 1 : 200 000 (1957) and Geological Map of the Murmansk region on a scale 1 : 2000000 (2001). (c) Geological scheme of the GDK northern segment and sampling localities.

METHODS

Petrographic studies of rocks and analysis of mineral composition were carried out with optical microscope and on a TESCAN Vega II LSH scanning electron microscope equipped with an EDS Inca Energy-350 at the Centre for Collective Use of the Karelian Research Center of the Russian Academy of Sciences (Petrozavodsk, CCU KarRC RAS). Minerals were analyzed in the carbon-coated (20 nm thick) polished thin sections at an accelerating voltage of 20 kV, a beam current of 15 nA ± 0.05 nA, a working distance of 15 mm, and counting time of 70 s. X-ray spectra were processed by optimization over spectra of standards of rock-forming minerals. Measurement errors were <2 rel % for elements with concentrations >10 wt %; <5 rel % for elements with concentrations 5–10 wt %; and up to 10 rel % for elements with concentrations 1–5 wt %.

Contents of major elements were determined on a PW-2400 (Philips Analytical B.V.) X-ray sequential fluorescence spectrometer at the Institute of Geology of Ore Deposits, Geochemistry, Mineralogy, and Petrography, Russian Academy of Sciences (IGEM RAS), Moscow. The analysis was performed in glass discs obtained by fusion of 0.3 g sample powder with 3 g of lithium tetraborate. Loss on ignition were determined gravimetrically. Accuracy of the analysis was 1–5 rel % for elements with concentrations >0.5 wt % and up to 12 rel % for elements with concentrations <0.5 wt %.

Concentrations of trace and rare-earth elements were determined by ICP-MS on a Thermo Scientific

XSeries 2 instrument at the CCU KarRC RAS using the conventional technique (Svetov et al., 2015). Samples were digested in an acid mixture in open system. The accuracy of the analyses was monitored by the measurement of USGS (BHVO-2) and in-house (SGD-2A) standards. The measurement results are given in Supplementary[1] 1, ESM_1.xls.

The zircon was extracted by magnetic and density separation at the Laboratory of Mineral Analysis of the IGEM RAS. Baddeleyite was extracted following the water-based method (Söderlund and Johansson, 2002) at the IGEM RAS.

The Rb-Sr and Sm-Nd isotopic studies were carried out at the Laboratory of Isotope Geochemistry and Geochronology of IGEM RAS. The chemical preparation of samples for mass-spectrometric measurements was carried out following technique described in (Larionova et al., 2007). Measurements of Sr and Nd isotopic compositions were performed on a Sector 54 mass-spectrometer (Micromass, the UK) in a multi-dynamic mode using a three-filament ion source (Thirlwall, 1991). The uncertainty of $^{143}Nd/^{144}Nd$ ratio was determined to be less than $\pm 0.0022\%$ by measurement of Nd-IGEM in-house standard of 0.512400 ± 11 ($2\sigma_u$, N = 24), which corresponds to $^{143}Nd/^{144}Nd = 0.511852$ in the LaJolla Nd standard. The uncertainty of the $^{147}Sm/^{144}Nd$ ratio is estimated to be $\pm 0.3\%$ ($2\sigma_u$) based on the multiple analyses of BCR-1 standard. The $^{87}Sr/^{86}Sr$ ratio in the SRM-987 standard during measurements was 0.710242 ± 15 ($2\sigma_u$, N = 31). The error in $^{87}Rb/^{86}Sr$ was at 1%. The generally accepted rubidium decay constants (Villa et al., 2015) were used in calculations.

The U-Pb baddeleyite study was carried out at the Laboratory of Isotope Geology, Institute of Precambrian Geology and Geochronology RAS (IPGG RAS, St. Petersburg). Most transparent and homogenous baddeleyite crystals taken for geochronological studies were multiply treated in ethanol, acetone, 1 M HNO_3 and 1 M HCl to remove surface contamination. After each stage, the grains were washed in analytical grade pure water. The chemical digestion of baddeleyite was carried out following a modified Krogh technique (Krogh, 1973) in Teflon vessels loaded in the Parr bombs and spiked with ^{202}Pb-^{235}U solution immediately prior to digestion.

Isotope analyses were performed on a TRITON TI mass-spectrometer using ion counter. The measurement accuracy of U/Pb ratios and U and Pb contents was 0.5%. Total blank was 1–5 pg of Pb and 1 pg of U. Experimental data were processed using PbDAT (Ludwig, 1991) and ISOPLOT (Ludwig, 2003) software. Ages were calculated using generally accepted uranium decay constants (Steiger and Jäger, 1977). Corrections for common lead were applied according to the model of Stacey and Kramers (1975). All errors are given at 2σ level.

Zircon grains extracted from samples ("unknown") together with zircon standards (Pb/U, Temora (Black et al., 2003) and U, 91500 (Wiedenbeck et al., 1995)) were mounted in epoxy ("pellet", resin Buehler Epokwick®) and polished to approximately half thickness (diamond abrasive 3 μm). Then the pellet was washed from contamination and zircon was photographed in transmitted and reflected light, as well as (after gold sputtering) examined using BSE and cathodoluminescence detectors (SEM CamScan MX2500S, UK). Obtained microphotographs were used to select analytical points and to determine the zircon nature.

In-situ U-Pb analyses were performed on a SIMS SHRIMP-II ion microprobe at the Centre of Isotopic Research (CIR, Russian Geological Research Institute (St. Petersburg, CIR VSEGEI) in monocollector mode of scanning over masses in compliance with standard protocol (Larionov et al., 2004). The crater size was 25×20 μm. Ion currents were measured using SEM on nine mass stations ($^{196}Zr_2O$ for ^{254}UO, four mass spectra per one analysis). Each fourth measurement was carried out on a Pb/U Temora standard (1σ uncertainty of standard calibration in Supplementary 2, ESM_2.xlsx). Obtained analytical results were processed with Excel-2003 macros SQUID v2.50 (Ludwig, 2009) and ISOPLOT/Ex 3.75 (Ludwig, 2012), unradiogenic Pb was corrected using measured $^{204}Pb/^{206}Pb$ and model values (Stacey and Kramers, 1975), and the ages were calculated using decay constants (Steiger and Jäger, 1977). Dates discussed in the text are given with error of 2σ, and results of individual analyses in the tables are given with error of 1σ.

RESULTS

Geology and Petrography

The northern segment of the mafic dyke that exposed in the Medvezh'ya Bay area (Figs. 1b, 1c) is traced by strike for over 1 km and is ~ 200 m thick. In this area mafic rocks form an NE-trending hill. The fine-grained dolerites are exposed in the western abrupt slope of the hill. This suggests the proximity of subvertical dyke contact, which is mostly overlain by Quaternary deposits. The eastern contact of the dyke is overlain by loose deposits, with rock shearing along the contact zone. The host rocks are represented by weakly gneissose medium-grained trondhjemites (sample Ca-812-16) in the east and by microcline granites (sample Ca-813-2) with up to 1 m enclaves of

[1] Supplementary to Russian and English on-line versions of paper are given at sites https://elibrary.ru/ and http://link.springer.com/ соответственно приведены:
Supplementary 1: ESM_1.xlsx—Results of measurement of standard samples;
Supplementary 2: ESM_2.xlsx—Compositions of minerals in GDK dolerites;
Supplementary 3: ESM_3.xlsx—U-Pb data on sample Ca-812-16;
Supplementary 4: ESM_4.xlsx—U-Pb data on sample Ca-554-3;
Supplementary 5: ESM_5.xlsx—Composition of host rocks.

mafic rocks in the west. The mafic rocks are massive, consist mainly of amphibole, plagioclase, biotite, and K-feldspar, and have the high contents of apatite and titanite. In the northern exposures, the GDK is intersected by a 1.5 m thick NE-trending (10°), 50° northwest dip dyke of amphibolitized fine-grained dolerites.

The GDK rocks preserved massive texture and are slightly schistose only in the eastern part of the body (sample Ca-812-1, 2) (Fig. 1c). The schistosity zones are filled by chlorite and carbonate, which indicates the low *P-T* parameters of transformations approximately corresponding to the greenschist facies. The latest stages of alteration are represented by thin prehnite–chlorite veins. Although in the most of studied samples from the eastern and central parts of the dyke, pyroxene is uralitized and amphibolized, and plagioclase is saussuritized or sericitized (Figs. 1c, 2), the studied samples, except for samples Ca-812-1, 2, retained relicts of primary clinopyroxene and plagioclase.

The dyke has a simple inner structure. Fine-grained poikilophitic dolerites that exposed near the western contact inward grade into the fine-grained poikilitic dolerites with scarce plagioclase phenocrysts up to 3 cm in size. To the center of the dyke, the grain size increases up to coarse-grained gabbrodolerites and pegmatoid varieties (samples Ca-812-3, 4; Figs. 1c, 2b, 2c). The studied GDK segment shows no macroscopic signs of in situ differentiation like layering or sharp changes in rock composition. Instead, equigranular massive dolerites and gabbro are predominant (Figs. 1c, 2).

Based on the relict mineral assemblages, the rocks are defined as gabbro and less common olivine-bearing gabbro. Clinopyroxene is usually uralitized and overgrown by hastingsite rim (Fig. 2d). Pyroxenes from gabbro, dolerites, and groundmass in the porphyritic varieties are weakly zoned and represented by augite. Pyroxenes vary in composition from X_{Mg} = 0.61–0.65 in the coarse-grained dolerites from central part to X_{Mg} = 0.65–0.69 in the marginal part of the dyke (Supplementary 3, ESM_3.xlsx). Clinopyroxene inclusions in the large plagioclase phenocrysts are represented by diopside (X_{Mg} = 0.61) and augite (X_{Mg} = 0.66) (Figs. 2b, 3a). All studied pyroxenes have the moderate concentrations of Al and Ti and low Na and Cr contents (Supplementary 2, ESM_2.xlsx).

Plagioclase composes up to 50 vol % of dolerites and gabbrodolerites, and forms large (up to 3 cm) phenocrysts in porphyritic rocks. In phenocrysts, plagioclase $An_{65–60}$ is highly sericitized and preserved only in rare relict domains (Figs. 2g, 2h). Phenocrysts are unzoned, excluding the outer rims that are more sodic in composition (An_{50}). In other cases, plagioclase forms weakly zoned ($An_{57–45}$) large laths and tabular grains, and more sodic ($An_{35–30}$) small laths. Albite ($An_{4–8}$) crystallizes in the interstices. Olivine is not preserved in the rocks, but clinopyroxene oikocrysts in the rocks from the western part of the body contain small round inclusions (Fig. 2e) morphologically resembling altered olivine grains. In addition, the alteration products of Fe–Mg mineral, likely low-Mg (mg# <0.6) olivine, that are replaced mostly by iron oxides and preserved a relict intragrain fractures occur in the eastern part of the body (sample Ca-812-5, 8). Biotite, whose content is several percent, forms single relict grains in a weakly altered rocks in the central part of the body. In the amphibolitized varieties, biotite forms rim around ore minerals and is crystallized together with metamorphic amphibole. Ore phases are dominated by Ti-V magnetite with large ilmenite lamellae. In plagioclase phenocrysts and large pyroxene grains, ore phase is represented by ilmenite with single lamellae of iron oxides. Chalcopyrite forms euhedral grains in the interstices of large plagioclase laths. Accessory apatite, baddeleyite, and zircon crystallized in interstices together with quartz, apatite, and biotite. Zircon forms large euhedral highly metamict grains in the pegmatoid varieties (Figs. 4a, 4b). Baddeleyite occurs as well preserved euhedral transparent and translucent grains, sometimes with zircon rims (Figs. 4c, 4d).

Results of U-Pb Geochronologcial Studies

Great Dyke of the Kola Peninsula. Over 200 baddeleyite grains 30–100 μm in size were extracted from the coarse-grained dolerite sampled in the central part of the body (sample Ca-812-4, Fig. 1c). Baddeleyite forms tabular and pseudoprismatic crystals of light brown to dark brown color. Some crystals are fringed by rims of transparent zircon.

U-Pb geochronological studies were performed for four microsamples (1–6 crystals) of the best preserved baddeleyite. As seen in Table 1 and Fig. 5a, the baddeleyite is concordant or is slightly discordant (1.6–4.8%), which is caused by the presence of submicron zircon rims formed by alteration processes. The concordant age of the baddeleyite is 2680 ± 6 Ma, MSWD = 0.26, and concordance probability of 0.61. This age coincides with the upper intercept age of 2686 ± 6 (MSWD = 1.9) obtained for all points of isotopic composition, while the lowest intercept gives the value of 1150 ± 130 Ma.

Trondhjemite, sample Ca-812-16. Zircon extracted from the trondhjemite sample collected near the eastern contact of the dyke (Fig. 1c) is represented by sub- and euhedral prismatic and elongate prismatic crystals with smoothed edges. In the transmitted light, the crystals are fractured, frequently show concentric growth zoning, and contain few inclusions. Cathodoluminescence (CL) studies demonstrate thin oscillatory zoning and frequently are mantled by low-luminescence rims.

U-Th-Pb geochronological studies (SHRIMP-II) were carried out for cores and rims of ten zircon grains.

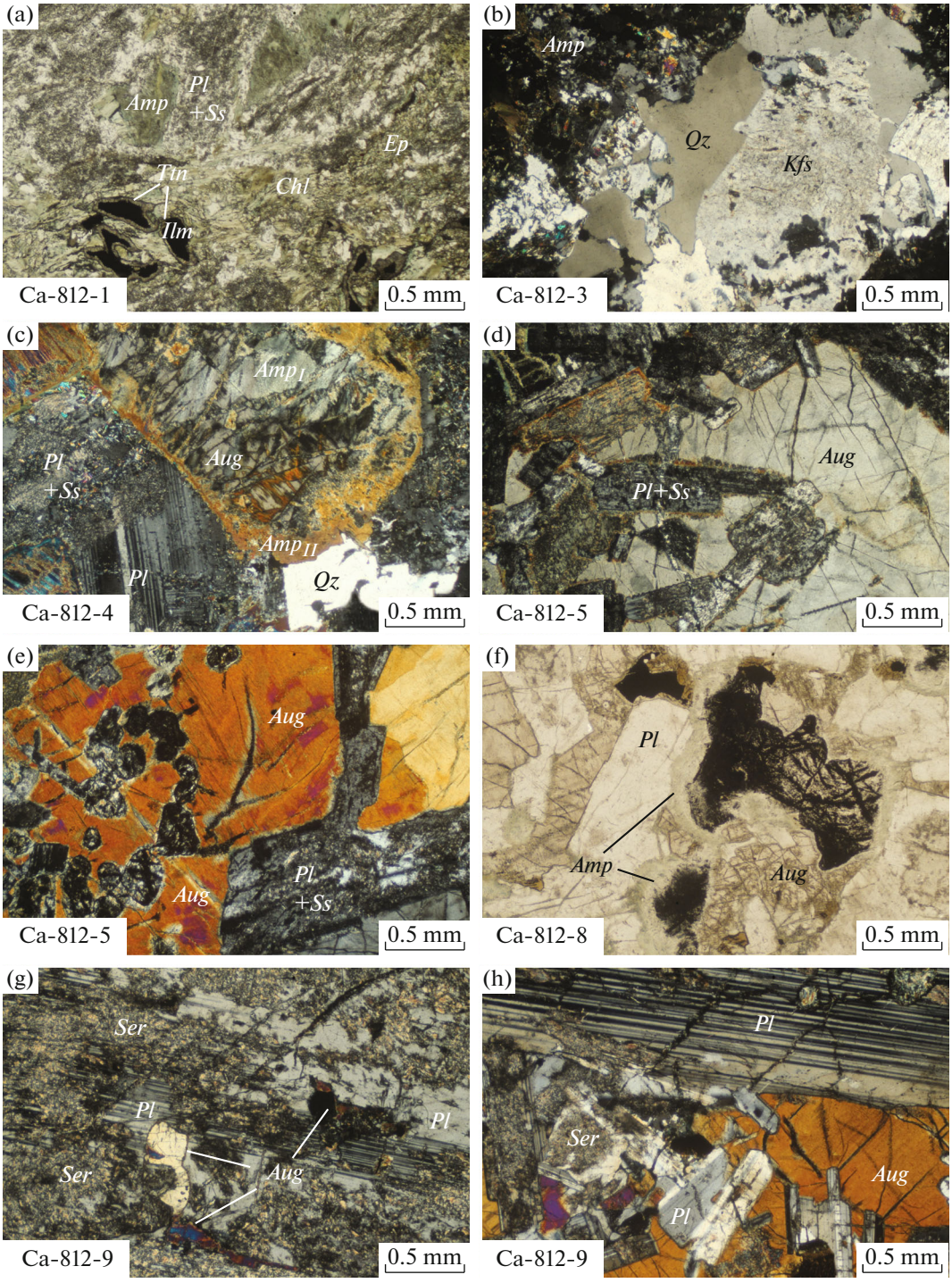

Fig. 2. Photos of polished thin sections of GDK rocks. (a) metamorphosed dolerite in the eastern part of the body; (b) quartz and K-feldspar in interstices between large grains of amphibolized pyroxenes in pegmatoid dolerites; (c) relicts of augite and plagioclase in pegmatoid dolerites from the central part of the body, from which baddeleyite was extracted; (d) relict augite grains in coarse-grained dolerites. Round inclusions in the augite are mainly made up of iron oxides; (e) augite oikocrysts in coarse-grained dolerites containing laths of highly altered plagioclase; (f) dolerite with large grain of replaced olivine (?) surrounded by amphibole rim. Black in the photo are iron oxides; (g) augite inclusions in the central part of large plagioclase phenocrysts in dolerites from the western part of the body; (h) rim of the large plagioclase phenocrysts in host poikilophitic dolerites. Mineral abbreviations are after (Warr, 2021), (*Ss)* saussurite, (*Ser)* sericite.

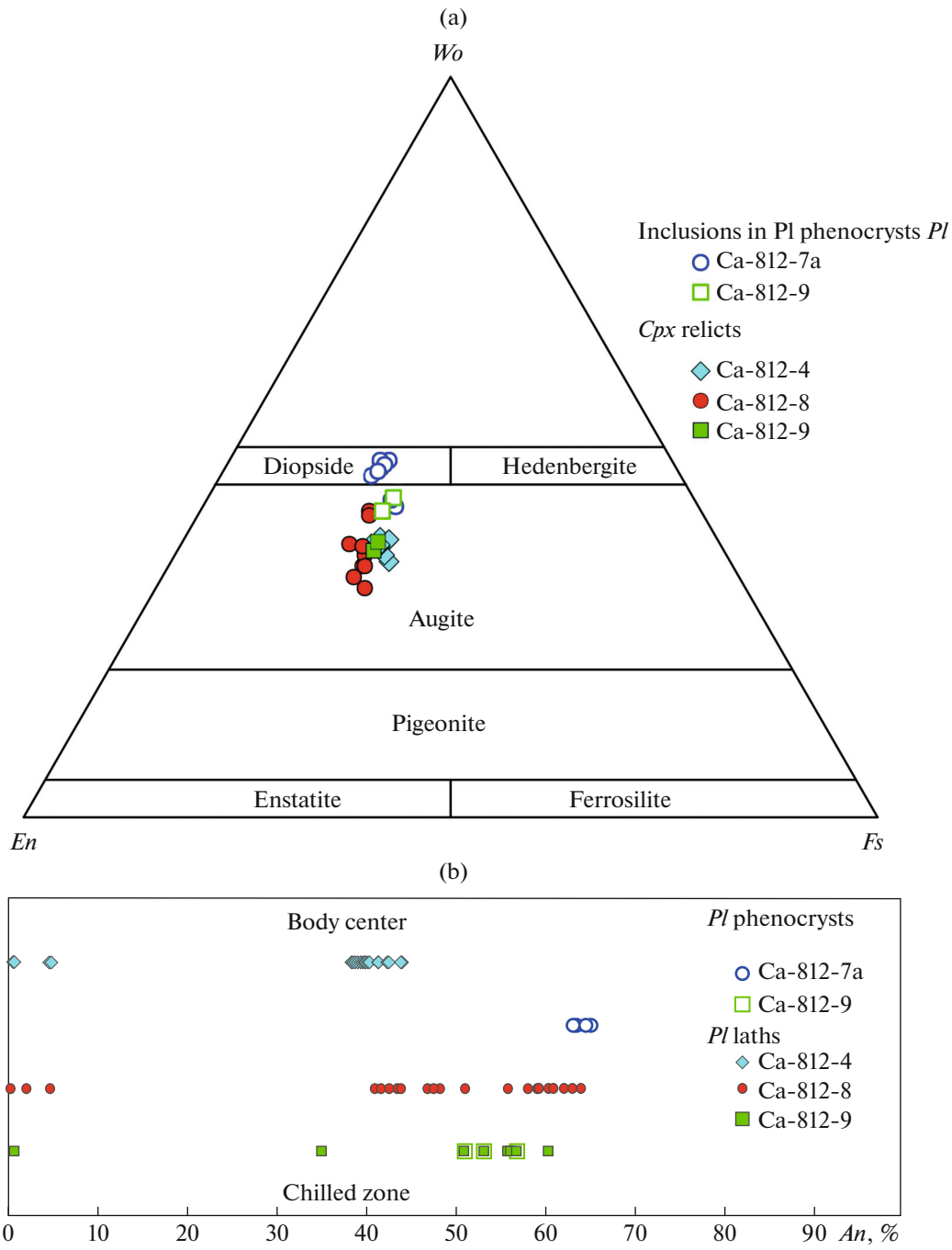

Fig. 3. Variations in composition of clinopyroxene and plagioclase in the GDK rocks. (a) position of data points of clinopyroxenes in the diagram wollastonite (*Wo*)–enstatite (*En*)–ferrosilite (*Fs*) (Morimoto et al., 1988), (b) variations of plagioclase composition, *An*, % is the content of anorthite end member.

Two CL-different rims (growth zones) are distinguished in some crystals (e.g., grain 4 in Figure and Supplementary 3, ESM3.xlsx). Most of obtained U-Pb results are highly discordant, and only four analyses yielded concordant ages, two of which were obtained for cores of zoned zircon, with the weighted average age ($^{207}Pb/^{206}Pb$) of 2.75 Ga (Supplementary 2, ESM_2.xlsx, Fig. 5b). Two other concordant $^{207}Pb/^{206}Pb$ ages <2.72 Ga were obtained for zircon domains showing no well expressed zoning (one rim and one core) (Supplementary 2, ESM_2.xlsx, Fig. 5b). Numerous fractures in the zircons could be the channels for diffusion of radiogenic Pb, which explains the deviation of almost half results (including those obtained from central domains with growth zoning) from ideal regression line (MSWD for all results ~6).

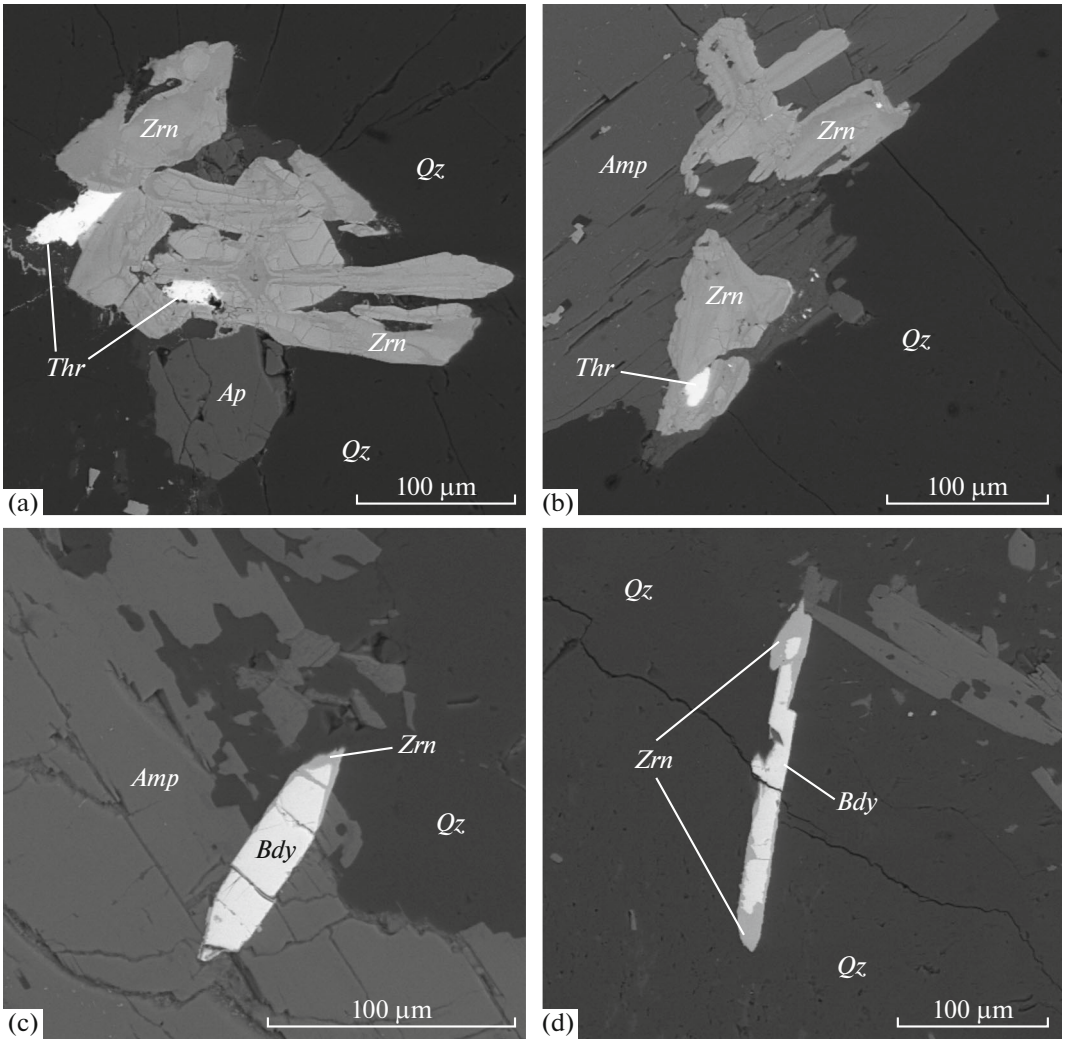

Fig. 4. Microphotographs of zircon and baddeleyite in the pegmatoid dolerites (sample Ca-812-3) (scanning electron microscope, BSE image). Metamictic zircon with thorite inclusions in quartz (a) and amphibole (b). Baddeleyite with traces of zircon replacement (c, d). Mineral abbreviations are after (Warr, 2021).

Thus, the age value obtained for unzoned zircons can be defined by Pb loss rather than reflects the age of geological process. The two concordant points of cores (6.1, 3.1) define an $^{207}Pb/^{206}Pb$ age of 2747 ± 9 Ma, while age of rims (4.2, 10.1) corresponds to 2711 ± 9 Ma (Fig. 5b, Supplementary 3, ESM_3.xlsx).

Trondhjemite, sample Ca-554-3. Trondhjemite sample Ca-554-3 taken east of the GDK, in the area of the Dal'nie Zelentsy settlement, yielded subeuhedral and euhedral, bipyramidal-prismatic transparent pale pink zircons. The most of zircons are fractured, frequently with large (up to 30–50 μm) polyphase and homogenous melt (?) inclusions. Three of 78 grains supposedly contain inherited cores. The growth zoning is poorly expressed due to the low cathodoluminescence (CL) intensity, but some grains have clear concentric oscillatory and sectorial zoning, which indicates a magmatic nature of the zircons. The low CL intensity is likely caused by the disturbance of structure (metamictization) and possible presence of admixtures. These features together with abundance of inclusions and high aspect ratio of grains (K_{el} = 2.5–4) suggest their rapid growth and could indicate the crystallization of this zircon at the late magmatic stage. This zircon has the elevated uranium content (300–4650 ppm) (Supplementary 4, ESM_4.xlsx). Most of analyzed grains (9 of 13) gave highly discordant U-Pb ages ($D > 7\%$) and are not approximated by a single regression line (MSWD = 65). The ages, depending on the analytical points selection, vary from 2730 ± 11 Ma (two most concordant results) to 2740 ± 8 Ma (MSWD = 1.9, six results) (Fig. 5c, Supplementary 4, ESM_4.xlsx). Given that inferred inherited cores were not analyzed, the oldest of these boundary age estimates (with least Pb loss) considered to be preferable.

Table 1. Results of U-Pb isotopic studies of baddeleyite from GDK dolerites

Ordinal no.	Size fraction (μm) and characteristics (color and habit)	U/Pb*	Pb_c/Pb_t	Isotope ratios					Rho	Age, Ma		
				$^{206}Pb/^{204}Pb^a$	$^{207}Pb/^{206}Pb^b$	$^{208}Pb/^{206}Pb^b$	$^{207}Pb/^{235}U$	$^{206}Pb/^{238}U$		$^{207}Pb/^{235}U$	$^{206}Pb/^{238}U$	$^{207}Pb/^{206}Pb$
1	>45, 6 grains, light-brown, platy	2.1	0.01	904	0.1777 ± 4	0.0132 ± 2	11.6277 ± 383	0.4746 ± 11	0.73	2575 ± 7	2504 ± 6	2631 ± 4
2	>45, 5 grains, light-brown, platy	2.0	0.07	337	0.1798 ± 3	0.0146 ± 2	12.0859 ± 495	0.4874 ± 18	0.92	2611 ± 10	2560 ± 9	2651 ± 3
3	>45, 3 grains, dark-brown, platy	1.7	0.09	271	0.1825 ± 2	0.0211 ± 2	12.6984 ± 253	0.5046 ± 8	0.89	2658 ± 5	2634 ± 5	2675 ± 2
4	>45, 1 grains, dark-brown, platy	1.9	0.007	406	0.1830 ± 3	0.0046 ± 2	12.9903 ± 780	0.5147 ± 20	0.92	2679 ± 16	2677 ± 13	2681 ± 4

* Baddeleyite aliquot was not determined; (Pb_c) common lead; (Pb_t) total lead; [a]measured isotope ratios; [b]isotope ratios corrected for blank and common lead; (Rho) error correlation coefficient of $^{207}Pb/^{235}U$–$^{206}Pb/^{238}U$. Errors (2σ) correspond to last digits.

Geochemistry and Sr-Nd Isotope Systematics

The GDK dolerites indicate tholeiitic series affinity (Fig. 6). They have low Mg number values (Mg# = 16–37) and MgO content from 7 wt % in the marginal zone to 3 wt % in gabbro-pegmatites (Table 2). The CaO, Cr, and Ni contents positively correlate with MgO, whereas Fe_2O_3, TiO_2, Zr, Rb and other incompatible elements negatively correlate with MgO (Fig. 7). The rocks containing plagioclase phenocrysts are enriched in Al_2O_3 (up to 16.7 wt %) (Table 2), while the most evolved rocks are enriched in Fe and Ti. All studied rocks have LREE enriched patterns ($(La/Sm)_n$ = 2.1–2.6), weakly fractionated HREE patterns ($(Gd/Yb)_n$ = 1.1–1.7), and negative HFSE anomalies, most expressed for niobium: Nb/Nb* = 0.19–0.25 (Fig. 8a, Table 2).

Host granitoids correspond to trondhjemites and granites and are similar to granitoids from the western part of the Murmansk Craton (Kozlov et al., 2006). Mafic enclaves correspond to the mild-alkaline medium-Mg (MgO = 6.5 wt %) basalts with high P_2O_5 content, extremely high concentrations of most incompatible elements, and sharp negative Eu and HFSE anomalies (Fig. 8, Supplementary 5, ESM_5.xlsx).

The GDK mafic rocks collected from different parts of the dyke have narrow variations of $\varepsilon_{Nd}(2680)$ values from –0.14 to +0.56 (Table 3), while initial Sr isotopic composition varies in a wide range giving $(^{87}Sr/^{86}Sr)_{2680}$ values of 0.7000–0.7075 (Table 4).

Compared to the mafic rocks, the granitoids eastward and westward of GDK have lower ε_{Nd} values from –0.13 to –0.84 and $(^{87}Sr/^{86}Sr)_{2680}$ from 0.6993 in trondhjemite to 0.7049 in granite (calculated for the dyke emplacement age of 2680 ± 6 Ma) (Tables 3, 4).

DISCUSSION

The Age and Position of the GDK in the Evolution of the Murmansk Craton

The robust age of GDK emplacement determined by baddeleyite dating is 2680 ± 6 Ma. The age of host granites is less definite. In the trondhjemite, zircon lost most of radiogenic lead and only a few well-preserved domains yielded two age estimates. The older age value of 2.75 Ga likely corresponds to the trondhjemite protolith age and defines the age of magmatic crystallization. The younger age value of 2.72 Ma obtained on unzoned rims and cores remains uncertain due to the possible lead loss. The younger age value probably corresponds to the endogenous reworking of protolith caused by injection of late two-feldspar granites, which are widespread in the region and terminate the Neoarchean acid magmatism in the western part of the Murmansk Craton, or likely indicate a thermal reworking due to emplacement of mafic dykes.

The GDK mafic rocks differ from mafic enclaves in granites, first of all, in the lower contents of trace and rare-earth elements (Figs. 7, 8). They also differ from metabasalts of the Ura-Guba–Kolmozero–Voron'ya greenstone belt (Vrevsky, 2018). The mafic rocks of the greenstone belts are high-magnesian, and with significantly lower trace elements concentrations than in the GDK dolerites (Fig. 8). Such compositional differences indicate that the GDK rocks were formed during a distinct episode of Archean mafic magmatism in the Murmansk Craton. Mafic enclaves that are similar in morphology and composition to enclaves in host granites are widespread in the Murmansk Craton (Kozlov et al., 2006 and our data). In some areas, such enclaves are concentrated around small mafic massifs or form chains along the strike of mafic dykes. The morphological features of the mafic enclaves, their ubiquitous association with granites (Kozlov et al., 2006), and enriched chemical composition typical of sanukitoid series rocks (Larionova et al., 2007) may indicate a simultaneous injection of mafic and felsic melts without magma mixing, i.e., mingling (Wilcox, 1999). In the Phanerozoic, such processes are most typical of post-collisional settings during collapse of collisional orogens (Sklyarov and Fedorovsky, 2006).

New and previously available age data on 2.72–2.75 Ga granites in other parts of the Murmansk Cra-

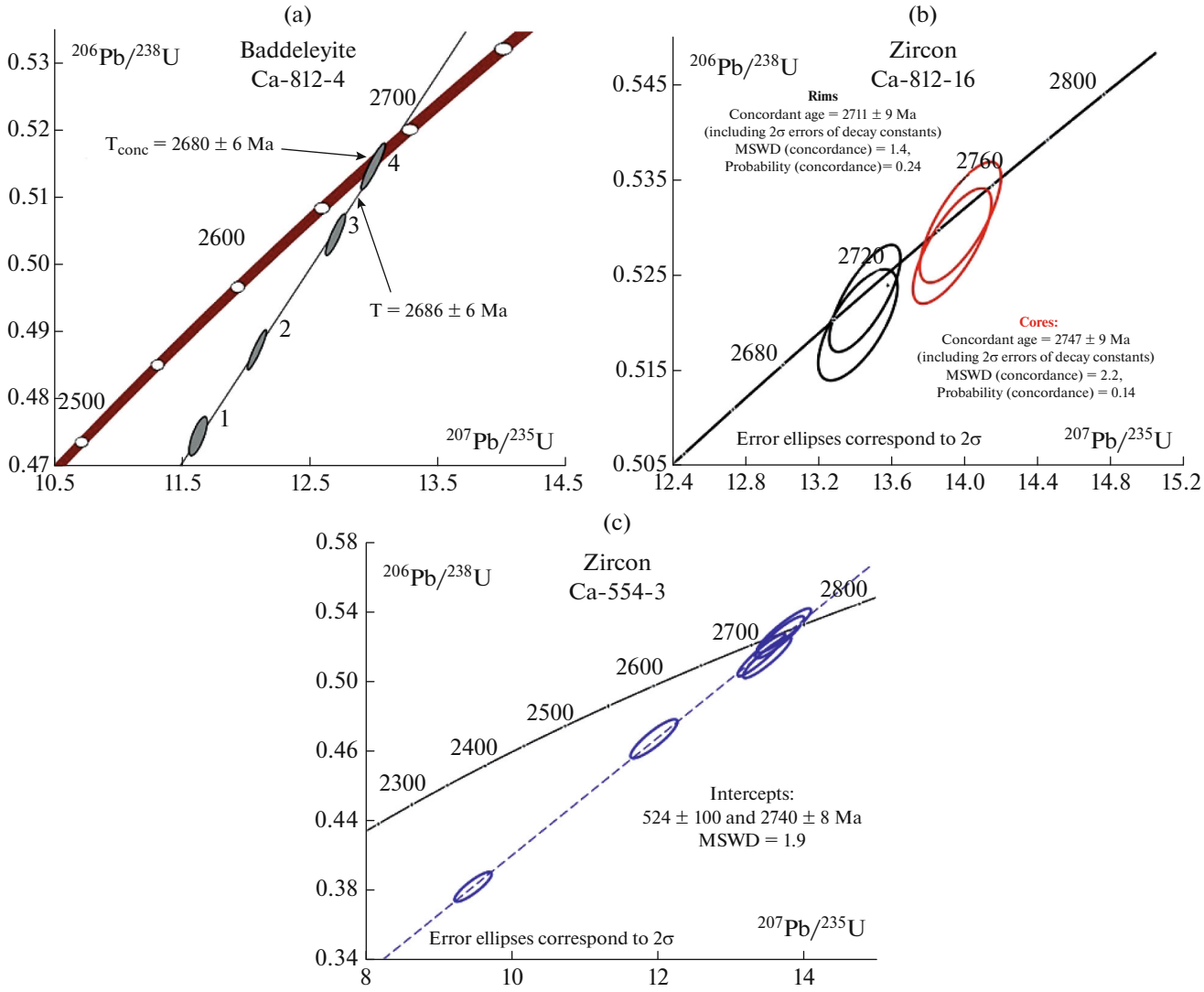

Fig. 5. Concordia diagrams showing the results of U-Pb geochronological studies: (a) baddeleyite (ID-TIMS method) from the GDK dolerites, sample Ca-812-4; (b) zircon (SIMS, SHRIMP-II) from trondhjemite, sample Ca-812-16; (c) zircon (SIMS, SHRIMP-II) from trondhjemite, sample Ca-554-3.

ton (Kozlov et al., 2006) indicate a relatively narrow, from 20 to 50 Ma, age interval between termination of crust-forming processes in the Murmansk craton and the GDK emplacement. Significant thickness and length of GDK reflect the high intensity of extension, while the presence of chilled rocks in the contact zone of the body indicates a significant temperature gradient between GDK magmas and host granitoids. The emplacement of large mafic dykes immediately after main crust-forming event is often recognized in the Precambrian shields. The Great Dyke of Zimbabwe is considered to be a marker of termination of the crust-forming processes in the Zimbabwe Craton (Oberthür et al., 2002). The crustal stabilization and termination of crust-forming processes are also marked by the Neoarchean mafic dykes in the North China and Yilgarn cratons (Li et al., 2010; Stark et al., 2018).

In Situ Evolution of the GDK Mafic Melt

Despite the widespread amphibolization of pyroxene and saussuritization of plagioclase, most part of the rocks retained relicts of primary minerals and textures (Fig. 2). The rocks also retained geochemical and isotopic characteristics. The exception is sheared and chloritized metamafic rocks near the eastern contact of the dyke (sample Ca-812-1, Fig. 2a). In these rocks, the alteration is expressed in a decrease of K_2O and Rb contents and in insignificant unsystematic variations of initial strontium isotopic composition, which indicate a disturbance of Rb-Sr isotope system (Tables 2, 3).

Gradual changes of rock composition from dyke margin to its center, the absence of the inner chilled zones and other evidence for multiple melt injection

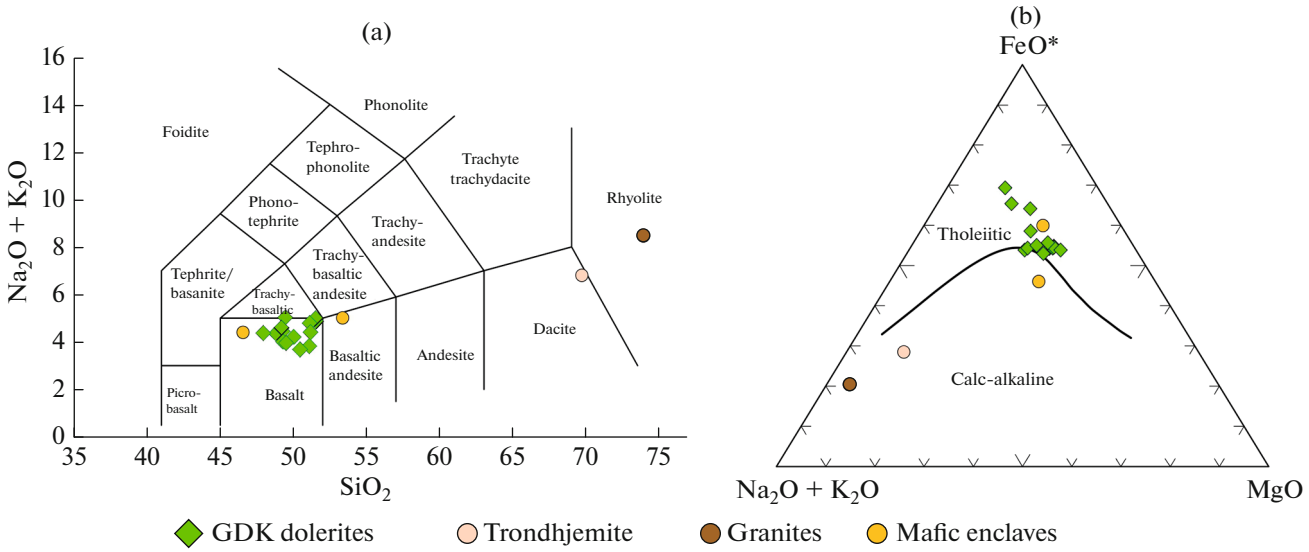

Fig. 6. Position of the GDK dolerites, host granitoids, and mafic enclaves on the classification diagrams. (a) TAS diagram (Le Bas et al., 1986), (b) AFM diagram (Irvine and Baragar, 1971).

indicate that the GDK was formed through a single magma injection. The crystallization of this large magma volume was accompanied by in situ differentiation, but its degree was insignificant: the rocks show no layering and cumulate textures typical of fractional crystallization. At the same time, in situ differentiation resulted in high concentrations of incompatible elements in the low-Mg rocks from the central part of the body (Figs. 7, 8), which is related to their accumulation in residual melts. The increase of Al_2O_3 in some samples is mainly caused by the presence of plagioclase phenocrysts in the rocks.

Chilled and marginal zones of the dyke correspond to the composition of melts that were supplied into a chamber. Based on the rock compositions, these melts had the low Mg number (Mg# = 37) and were not in equilibrium with mantle rocks. This suggests that primary melts were differentiated in intermediate chamber(s). The presence of plagioclase phenocrysts suggests a shallow-level position of the intermediate magma chamber (Presnall et al., 1978).

Composition of the GDK Sources

Petrography and chemical characteristics of rocks such as low MgO, Cr, and Ni contents indicate that GDK primary magmas experienced differentiation and do not represent melts that were in equilibrium with a mantle source. Based on phenocryst composition, differentiation occurred at least in two stages: in a feeding shallow magma chamber and in a deep-seated intermediate magma chamber, where main compositional features of the melts were formed.

Obtained geochemical data give restrictions on the composition of primary magmas. The mafic rocks with the highest Mg content in the GDK display very weakly fractionated HREE patterns ($(Gd/Yb)_n = 1.2–1.3$) suggesting the generation of primary melts via melting of a garnet-free source at a depth less than 60 km. Enriched LREE patterns along with deep negative Nb anomalies and moderately radiogenic neodymium isotopic composition (Table 3, Fig. 9) indicate a contribution of an ancient enriched lithospheric source, which could be represented by Archean granitoids and/or lithospheric mantle enriched in incompatible elements via subduction reworking. The same conclusions were obtained from Ti, Th, and Yb contents (Fig. 10). The Th/Nb ratio allows one to estimate crustal and (or) lithospheric contribution, while TiO_2/Yb ratio indicates the presence of garnet in a source and melting depth. A combination of these parameters reflects a contribution of plume and lithospheric sources in the melt origin (Pearce et al., 2021). The GDK composition points in Fig. 10 fall into SZLM (subduction zone-modified lithospheric mantle) field suggesting the input of sublithospheric mantle and enriched subcontinental lithospheric mantle sources in primary melts.

Generation of primary GDK melts at shallow depths in equilibrium with garnet-free residue, which is indicated by the low $(Gd/Yb)_n$ and TiO_2/Yb ratios, suggests the involvement of shallow asthenospheric source. Enriched lithospheric source, which produced mafic rocks associated with granites prior to GDK emplacement could be considered as a SZLM component. It should be emphasized that studied mafic rocks of small enclaves in the host granites likely experienced significant alteration due to interaction with ambient granite melt, and their geochemical signatures are not typical of SZLM (Fig. 11b). The better

Table 2. Chemical composition of GDK rocks

Components	Ca-812-1	Ca-812-2	Ca-812-3	Ca-812-4	Ca-812-5	Ca-812-6	Ca-812-7	Ca-812-8	Ca-812-9	Ca-812-10	Ca-812-11	Ca-812-14	Ca-812-15
	1	2	3	4	5	6	7	8	9	10	11	12	13
SiO_2	47.65	48.27	50.72	48.10	49.66	48.61	47.97	48.52	46.98	47.39	50.20	49.87	49.90
TiO_2	1.33	2.01	2.34	1.94	1.17	1.19	0.98	0.98	1.15	1.09	1.09	1.15	1.18
Al_2O_3	16.32	14.59	12.95	12.71	13.87	14.25	16.42	16.64	16.15	16.65	15.40	15.61	14.83
Fe_2O_3	13.21	16.46	17.66	16.83	12.63	12.72	12.74	12.96	14.09	12.17	11.60	11.66	12.09
MnO	0.23	0.27	0.27	0.26	0.20	0.21	0.18	0.18	0.19	0.17	0.18	0.18	0.20
MgO	5.03	3.78	3.01	5.10	6.66	6.64	6.79	6.91	6.90	6.36	5.06	5.12	5.58
CaO	8.40	7.02	6.41	9.09	9.30	9.35	8.16	7.79	7.88	7.88	9.02	9.27	9.44
Na_2O	3.76	3.77	3.77	3.15	2.95	3.22	3.01	2.98	3.27	3.59	3.43	3.35	3.21
K_2O	0.54	1.14	1.03	1.14	0.78	0.87	0.90	0.91	1.02	0.84	1.44	1.34	1.10
P_2O_5	0.19	0.30	0.41	0.17	0.15	0.15	0.14	0.16	0.17	0.16	0.20	0.16	0.16
L.O.I.	3.08	2.18	1.14	1.31	2.42	2.62	2.53	1.79	1.98	3.47	2.18	2.06	2.10
Total	99.74	99.79	99.71	99.80	99.79	99.83	99.82	99.82	99.78	99.77	99.80	99.77	99.79
Li	12.2	12.2	7.4	5.7	12.5	16.2	10.9	7.4	9.2	21.0	11.0	10.5	14.1
V	278	439	405	384	258	246	170	172	176	167	223	227	248
Cr	60.5	27.2	10.3	33.7	201	185	80.1	60.3	50.9	47.0	94.4	97.7	121
Co	54.0	47.0	45.2	59.7	56.3	52.9	65.1	70.2	68.5	64.0	44.6	42.6	44.4
Ni	74.9	34.7	17.2	64.0	83.2	76.4	147	167	165	154	62.5	54.8	59.8
Cu	104	129	99.6	228	90.2	83.4	77.2	84.7	90.9	89.1	63.2	76.8	78.7
Zn	136	185	183	128	99.0	94.76	95.3	102	106	101	97.2	92.8	94.9
Rb	22.2	48.7	33.3	27.1	20.8	22.5	25.0	28.4	28.9	23.1	39.6	33.4	27.5
Sr	469	333	223	248	304	310	332	340	352	370	344	316	305
Y	17.5	29.7	41.1	21.8	19.3	18.1	13.6	14.2	14.7	14.3	18.6	16.3	17.0
Zr	58.2	105	196	64.0	66.4	64.4	62.7	68.2	70.4	70.9	72.7	68.6	63.3
Nb	4.18	7.03	10.2	3.75	2.89	2.80	2.66	2.75	3.13	2.97	3.57	2.79	2.77
Ba	175	409	766	446	314	334	313	358	397	333	681	559	578
La	14.8	23.8	34.2	14.3	12.2	12.3	11.5	12.0	13.1	12.1	15.2	12.0	11.9
Ce	31.0	50.8	73.1	23.6	20.3	20.5	19.0	19.9	21.7	21.4	25.3	21.0	20.9
Pr	3.86	6.42	8.86	4.04	3.52	3.49	3.14	3.22	3.47	3.29	4.15	3.31	3.27
Nd	15.7	25.4	36.1	17.8	15.3	15.0	13.4	13.6	14.8	14.3	17.4	14.3	14.4
Sm	3.63	5.75	8.10	4.21	3.68	3.62	3.00	3.09	3.25	3.13	3.97	3.28	3.39
Eu	1.30	1.88	2.67	1.64	1.24	1.28	1.14	1.17	1.21	1.16	1.37	1.27	1.26
Gd	3.83	6.15	8.50	4.44	3.94	3.83	3.10	3.21	3.32	3.23	4.09	3.44	3.61
Tb	0.56	0.89	1.27	0.71	0.62	0.61	0.48	0.48	0.51	0.48	0.64	0.54	0.56
Dy	3.52	5.54	7.77	4.31	3.78	3.72	2.91	2.91	3.11	2.99	3.81	3.28	3.42
Ho	0.71	1.10	1.55	0.88	0.77	0.74	0.60	0.58	0.61	0.60	0.74	0.67	0.68
Er	2.04	3.19	4.52	2.52	2.21	2.18	1.68	1.72	1.80	1.73	2.24	1.96	2.01
Tm	0.29	0.46	0.65	0.47	0.41	0.38	0.31	0.30	0.32	0.30	0.37	0.33	0.33
Yb	1.85	2.93	4.11	3.13	2.71	2.59	1.99	2.01	2.06	1.94	2.49	2.10	2.12
Lu	0.27	0.42	0.60	0.36	0.31	0.31	0.24	0.24	0.26	0.25	0.32	0.28	0.29
Hf	1.45	2.62	4.51	1.64	1.79	1.69	1.50	1.65	1.64	1.64	1.95	1.77	1.67
Pb	17.73	9.86	10.92	7.44	6.72	4.70	4.15	4.05	4.16	4.37	4.79	4.21	6.04
Th	2.76	4.60	6.53	2.60	2.24	2.22	2.13	2.05	2.28	2.17	2.49	2.17	2.14
U	0.60	1.03	1.46	0.56	0.54	0.53	0.52	0.54	0.55	0.54	0.63	0.54	0.55
Mg#	0.30	0.20	0.16	0.25	0.37	0.37	0.37	0.37	0.35	0.37	0.33	0.33	0.34
Nb/Nb*	0.24	0.24	0.25	0.22	0.20	0.19	0.19	0.20	0.21	0.21	0.21	0.20	0.20

(1) Sheared metamorphosed dolerite, (2) coarse-grained gabbrodolerite, (3) coarse-graned gabbrodolerite; (4) coarse-grained gabbrodolerite, (5) metamorphosed gabbrodolerite, (6) gabbrodolerite, (7–9) *Pl*-porphyritic gabbrodolerite, (10) fine-grained dolerite, (11–13) gabbrodolerite. Mg# = $MgO/(MgO + FeO_{tot})$, $Nb/Nb^* = Nb_{PM}/(Th_{PM} \times La_{PM})^{1/2}$.

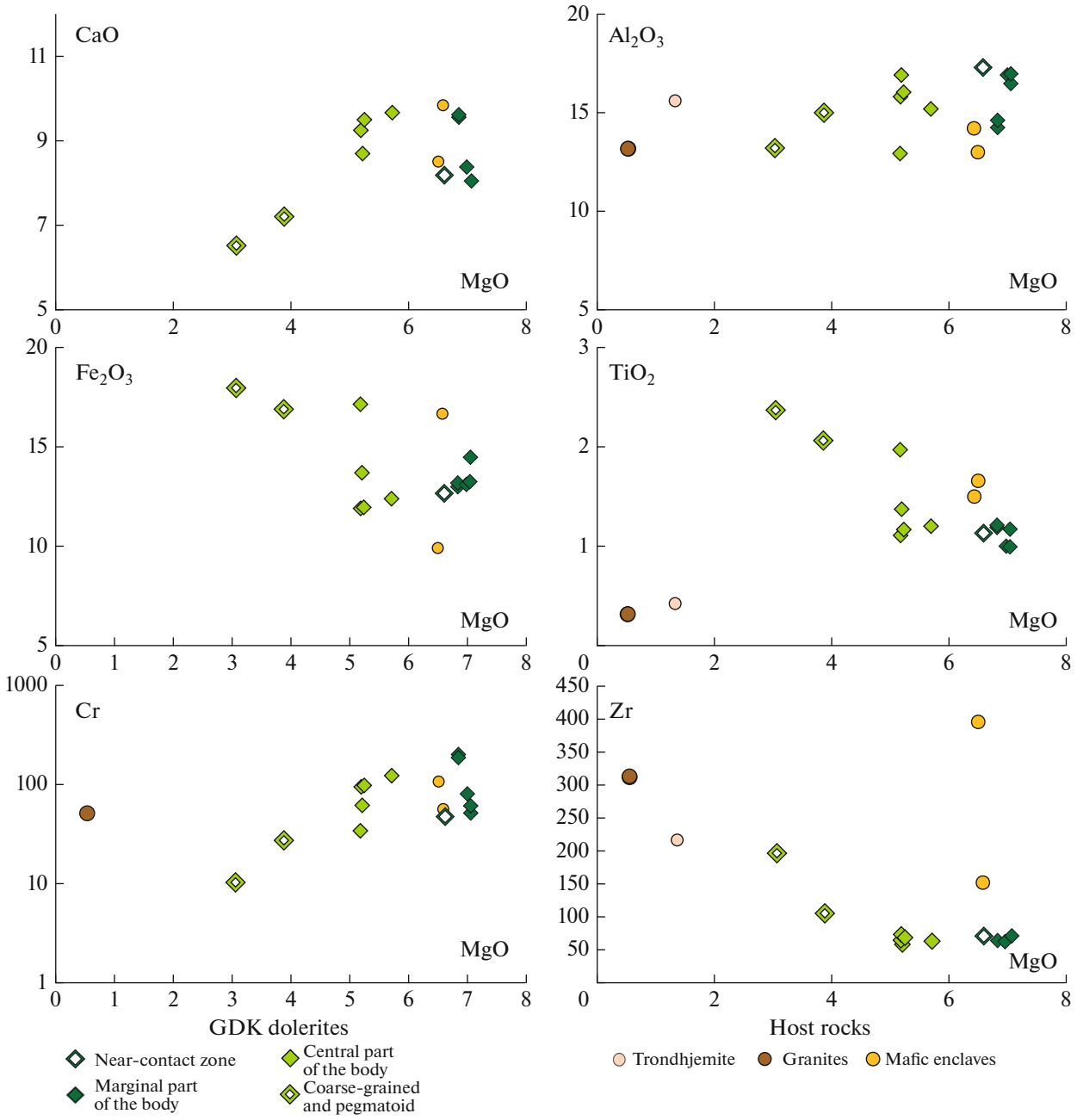

Fig. 7. Variations of major oxides, Cr and Zr versus MgO in the GDK dolerites, host granitoids, and mafic enclaves. Position of samples of the GDK dolerites within the body is shown by corresponding symbols in Fig. 1c.

preserved metamafic rocks and metadiorites with an age of 2.72 Ga that could be considered as derivates of enriched lithospheric mantle, occur in the central part of the Murmansk Craton in Litskiy Cape area (Samsonov et al., 2019).

Mass-balance calculations suggest that the most primitive GDK compositions could be obtained by mixing of 70% D-MORB asthenospheric melt (Klein, 2003) and 30% of melt derived via enriched lithospheric mantle melting (Fig. 11a). The Sm-Nd isotopic data give similar proportions of asthenospheric and lithospheric sources (Fig. 11b) (Supplementary 6, ESM_6.xls).

Pearce et al. (2021) suggest that melts with a SZLM signatures could be derived by the following mechanisms: (1) lithosphere delamination or (2) melting of SCLM affected by upwelling high-temperature deep-seated mantle plume. Obtained data and calculation results are consistent with a model of lithosphere delamination accompanied by mixing of asthenospheric and lithospheric melts of Wang and Currie (2015).

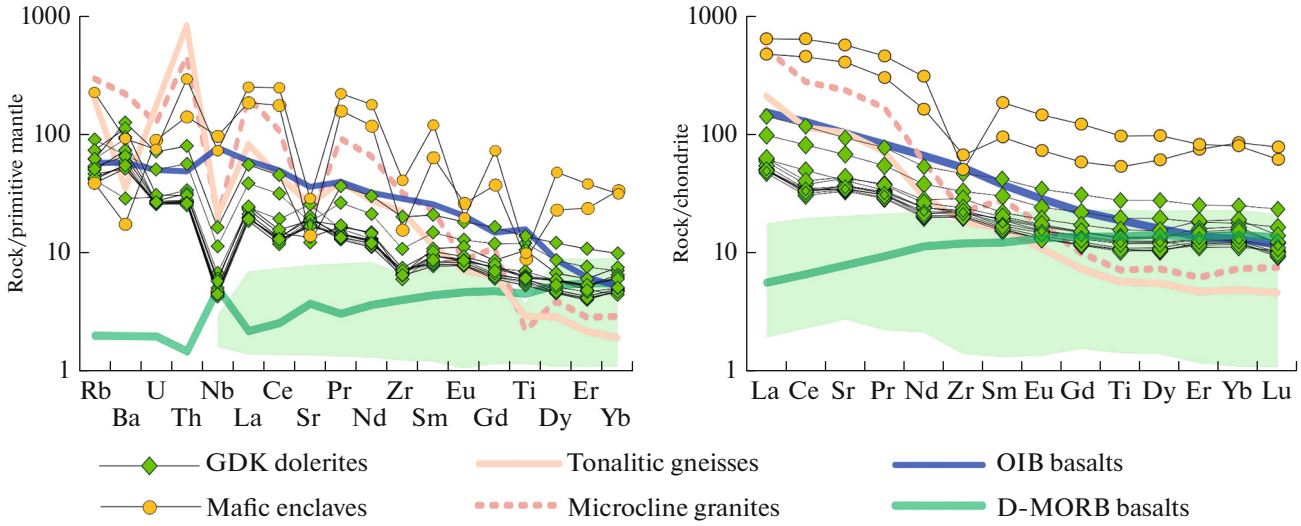

Fig. 8. Trace and rare-earth element distribution in the GDK dolerites, host granitoids, and inclusions in them, basalts and komatiites of Archean greenstone belts of the Kola–Norwegian province (green field, Vrevsky, 2018), D-MORB basalts (Klein, 2003), and OIB (Sun, McDonough, 1989). Normalization values after (McDonough and Sun, 1995).

Correlation of Neoarchean Dyke Magmatism in the Fennoscandian and Other Shields Worldwide

Although fifteen years ago the Neoarchean mafic dykes and large igneous provinces were practically unknown (Bleeker and Ernst, 2006), at present Neoarchean mafic dykes have been dated at many cratons worldwide. The GDK is close in age to the Stillwater layered intrusion and mafic dykes of the Wyoming Craton, which are ascribed to the Stillwater–Rendez-

Table 3. Sm-Nd isotope data on GDK mafic rocks and host granitoids

Sample no.	Rock	Sm	Nd	$^{147}Sm/^{144}Nd$	$^{143}Nd/^{144}Nd$	±2s	T*, Ma	$\varepsilon_{Nd}(T)$	T(DM)**
Ca-812-1	Sheared metadolerite	3.77	17.0	0.13423	0.511546	0.000006	2680	0.24	3060
Ca-812-4	Coarse-grained dolerite	3.46	14.9	0.14045	0.511672	0.000006	2680	0.56	3059
Ca-812-9	*Pl*-porphyritic dolerite	3.01	13.8	0.13183	0.511509	0.000007	2680	0.35	3039
Ca-812-10	Fine-grained dolerite	2.79	12.8	0.13197	0.511486	0.000007	2680	–0.14	3085
Ca-812-16	Trondhjemite	3.94	27.8	0.08552	0.510629	0.000005	2750	0.17	2980
Ca-813-2	Granite	7.61	63.7	0.07216	0.510429	0.000005	2720	0.52	2913

* Age according to U-Pb baddeleyite and zircon dating (see text).
** Model age relative to depleted mantle (Goldstein and Jacobsen, 1988).

Table 4. Rb-Sr isotopic data on GDK mafic rocks and host granitoids

Sample no.	Rock	Rb	Sr	$^{87}Rb/^{86}Sr$	$^{87}Sr/^{86}Sr$	±2s	T*, Ma	$(^{87}Sr/^{86}Sr)_T$
Ca-812-1	Sheared metadolerite	21.7	483	0.1301	0.712510	0.000015	2680	0.707462
Ca-812-4	Coarse-grained dolerite	32.6	297	0.3171	0.713631	0.000010	2680	0.701333
Ca-812-9	*Pl*-porphyritic dolerite	34.1	386	0.2562	0.709973	0.000009	2680	0.700035
Ca-812-10	Fine-grained dolerite	27.7	402	0.1993	0.711212	0.000009	2680	0.703483
Ca-812-16	Trondhjemite	104	438	0.6846	0.725865	0.000014	2680	0.699310
Ca-813-2	Granite	108	300	1.0422	0.745344	0.000009	2680	0.704918

* Age according to U-Pb baddeleyite and zircon dating (see text).

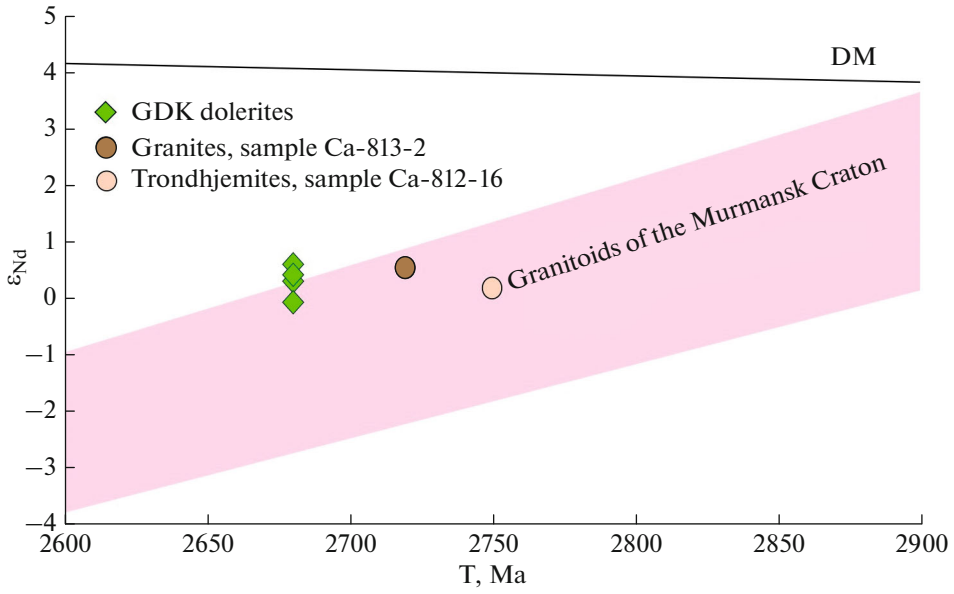

Fig. 9. Diagram ε_{Nd}–T for the GDK dolerites and host granitoids. Evolution field of the Nd isotopic composition for Archean gneisses and granitoids from the western Murmansk Craton was constructed using data (Timmerman and Daly, 1995; Kozlov et al., 2006; Pozhilenko et al., 2018). DM is the depleted mantle evolution curve after (Goldstein and Jacobsen, 1987).

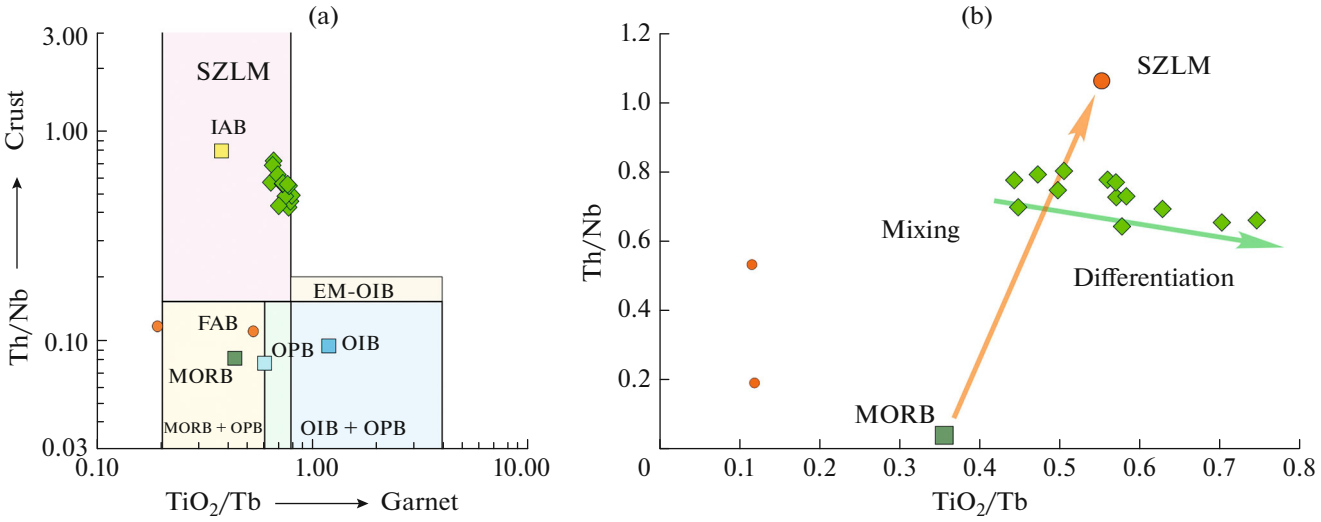

Fig. 10. (a) Position of data points of mafic rocks in the Pearce diagram (Pearce et al., 2021). (MORB) mid-ocean ridge basalts, (OPB) oceanic-plateau basalts, (OIB) ocean-island basalts, (IAB) island-arc basalts, (FAB) fore-arc basalts, (SZLM) subduction zone modified lithospheric mantle. (b) detail of Fig. (a). Hereinafter, data on MORB are taken from (Klein, 2003).

vous event in the Canadian Shield (Ernst et al., 2021). Dykes and sills of age 2.72–2.70 Ga occur at the Zimbabwe, Yilgarn, and Slave cratons, where they are regarded as components of the Goldfield Superior tholeiitic event (Hayman et al., 2015; Austin, 2022).

In the Karelian Craton, ca. 2.7 Ga mafic dykes have not been known yet. At the same time, mafic dykes (2670 ± 10 Ma, Balagansky et al., 1990) and intrusion (Suprotivnye Island, 2711 ± 25 Ma) (Slabunov et al., 2008) of similar age occur in the Belomorian Province. The available data are insufficient to estimate the scale of the ca. 2.7 Ga event in the Fennoscandian shield, but the presence of megadykes is one of the important criteria for recognizing the large

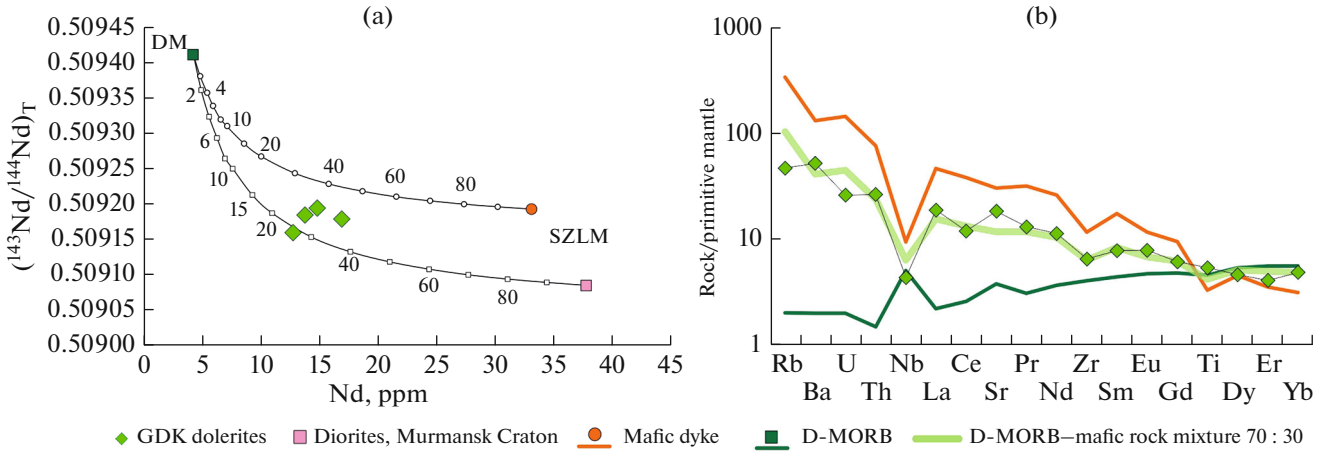

Fig. 11. Assessment of mixing parameters of melts formed through melting of depleted asthenospheric and enriched lithospheric sources compared to characteristics of the GDK mafic rocks based on the isotopic (a) and geochemical (b) data. A mixture of mafic rock–D-MORB is a result of mass-balance calculation of composition obtained by mixing of 70% D-MORB melt and 30% melt corresponding to the Neoarchean diorites of the Murmansk Craton. Initial compositions are given in Supplementary, ESM_6.xlsx.

igneous events (Ernst et al., 2021) that suggests the existence of the Neoarchean large igneous province in the northeastern Fennoscandian shield.

CONCLUSIONS

(1) Crystallization age of the Great Dyke of the Kola Peninsula determined by U-Pb (ID-TIMS) baddeleyite dating is 2680 ± 6 Ma. The U-Pb age of zircons from host granitoids (SHRIMP-II) is within 2.72–2.75 Ga.

(2) In the studied northern segment, the GDK consists of tholeiitic series low-Mg mafic rocks, has a simple structure, and was formed through a one-stage injection.

(3) The primary melts of the GDK could be formed via mixing of depleted asthenospheric and enriched lithospheric melts derived due to lithosphere delamination.

(4) The GDK marks the termination of Archean orogenesis and cratonization of the Neoarchean continental lithosphere in the northeastern Fennoscandian shield.

ACKNOWLEDGMENTS

Our studies were largely conducted owing to V.S. Kulikov, his encyclopedic knowledge and keen interest in the geology of Fennoscandia. Discussions on mafic dykes of the Fennoscandian Shield with V.S. Kulikov motivated us to study the Great Dyke of the Kola Peninsula, which is an important but forgotten for decades object. Our thanks for help in expedition works are addressed to the crew of the Udacha vessel O.U. Mingazov and G.I. Mukhin. Constructive comments of reviewers A.A. Nosova and N.M. Kudryashov significantly improved our manuscript.

FUNDING

The studies were supported by the Russian Science Foundation (project no. 16-17-10260P).

CONFLICT OF INTEREST

The authors declare that they have no conflicts of interest.

SUPPLEMENTARY INFORMATION

The online version contains supplementary material available at https://doi.org/10.1134/S086959112206008X.

REFERENCES

Arzamastsev, A.A., Fedotov, Zh.A., and Arzamastseva, L.V., *Daikovyi magmatizm severo-vostochnoi chasti Baltiiskogo shchita* (Dike Magmatism of the Northeastern Baltic Shield), Moscow: Nauka, 2009.

Austin, J.M., Hayman, P.C., Murphy, D.T., et al., The voluminous 2.81–2.71 Ga Goldfields tholeiitic super event: implications for basin architecture in the Yilgarn craton and global correlations, *Precambrian Res.,* 2022, vol. 369, 106528.

Balagansky, V.V., Bibikova, E.V., Bogdanova, S.V., et al., U-Pb geochronology of Belomorides of the Tupaya uba area, Lake Kovdozero, Northern Karelia, *Izv. AN SSSR, Ser. Geol.,* 1990, no. 6, pp. 40–51.

Balagansky, V.V., Glaznev, V.N., and Osipenko, L.G., The Early Proterozoic evolution of the northeastern Baltic Shield: a terrane analysis, *Geotectonics,* 1998, vol. 32, no. 2, pp. 81–92.

Balagansky, V.V., Mints, M.V., Daly, D.S., Paleoproterozoic Lapland–Kola orogen, *Stroenie i dinamika litosfery Vostochnoi Evropy. Rezul'taty issledovanii po programme EUROPROBE* (Structure and Dynamics of the Lithosphere of East Europe. Results of Studies in the Framework of EU-

ROPROBE Program), Moscow: Geokart, 2006, pp. 158–171.

Le Bas, M.J., Le Matre, R.W., Streckeisen, A., Zanettin, B.A., Chemical classification of volcanic rocks based on the total alkali–silica diagram, *J. Petrol.,* 1986, vol. 27, pp. 745–750.

Black, L.P., Kamo, S.L., Allen, C.M., et al., Temora 1: a new zircon standard for Phanerozoic U-Pb geochronology, *Chem. Geol.,* 2003, vol. 200, nos. 1–2, pp. 155–170.

Bleeker, W. and Ernst, R.R.E., Short-lived mantle generated magmatic events and their dyke swarms: the key unlocking earth's paleogeographic record back to 2.6 Ga, *Dyke Swarms—Time Markers of Crustal Evolution. Proceed. Fifth Int. Dyke Conference,* 2006, pp. 3–26.

Bogdanova, S.V., Gorbatschev, R., and Garetsky, R.G., *Europe|East European Craton*, *Reference Module in Earth Systems and Environmental Sciences,* 2016. https://doi.org/10.1016/B978-0-12-409548-9.10020-X

Bonin, B., Do coeval mafic and felsic magmas in post-collisional to within-plate regimes necessarily imply two contrasting, mantle and crustal, sources? A review, *Lithos,* 2004, vol. 78, no. 1, pp. 1–24.

Corfu, F., Hanchar, J.M., Hoskin, P.W.O., et al., Atlas of zircon textures, *Rev. Mineral. Geochem.,* 2003, vol. 53, pp. 469–499.

Cottin, J.Y., Lorand, J.P., Agrinier, P., et al., Isotopic (O, Sr, Nd) and trace element geochemistry of the Laouni layered intrusions (Pan-African Belt, Hoggar, Algeria): evidence for post-collisional continental tholeiitic magmas variably contaminated by continental crust, *Lithos,* 1998, vol. 45, nos. 1–4, pp. 197–222.

Daly, J.S., Balagansky, V.V., Timmerman, M.J., and Whitehouse, M.J., The Lapland–Kola orogen: Palaeoproterozoic collision and accretion of the northern Fennoscandian lithosphere, *Geol. Soc. London: Mem.,* 2006, vol. 32, pp. 579–598. https://doi.org/10.1144/GSL.MEM.2006.032.01.35

Daly, J.S., Balagansky, V.V., Timmerman, M.J., et al., Ion microprobe U-Pb zircon geochronology and isotopic evidence for a trans-crustal suture in the Lapland–Kola orogen, northern Fennoscandian Shield, *Precambrian Res.,* 2021, vol. 105, pp. 289–314. https://doi.org/10.1016/S03019268(00)00116-9

Ernst, R.E., *Large Igneous Provinces,* Cambridge: University Press, 2014.

Ernst, R.E. and Bell, K., Petrology of the great Abitibi dyke, Superior, *J. Petrol.,* 1992, vol. 33, no. 2, pp. 423–469.

Ernst, R.E., Liikane, D.A., Jowitt, S.M., et al., A new plumbing system framework for mantle plume-related continental large igneous provinces and their mafic-ultramafic intrusions, *J. Volcanol. Geotherm. Res,* 2019, vol. 384, pp. 75–84.

Ernst, R.E., Bond, D.P.G., Zhang, S., et al., *Large igneous province record through time and implications for secular environmental changes and geological time-scale boundaries, Large Igneous Provinces: A Driver of Global Environmental and Biotic Changes,* Wiley, 2021, pp. 1–26.

Fedotov Zh.A., Bayanova T.B., Serov P.A. Spatiotemporal relationships of dike magmatism in the Kola Region, the Fennoscandian Shield, *Geotectonics,* 2012, vol. 46, no. 6, pp. 412–426.

Geologiya SSSR. Murmanskaya oblast' (Geology of the USSR. Murmansk Region), Moscow: Gosgeoltekhizdat, 1958.

Goldstein, S.J. and Jacobsen, S.B., The Nd and Sr isotopic systematics of river-water dissolved material: implications for the sources of Nd and Sr in seawater, *Chem. Geol. Isot. Geosci. Sect.,* 1987, vol. 66, no. 3, pp. 245–272.

Halls, H.C., Hamilton, M.A., and Denyszyn, S.W., The Melville Bugt dyke swarm of Greenland: a connection to the 1.5–1.6 Ga Fennoscandian rapakivi granite province? *Dyke Swarms: Keys for Geodynamic Interpretation: Keys for Geodynamic Interpretation,* Srivastava, R.K., Ed., Berlin–Heidelberg: Springer Berlin Heidelberg, 2011.

Hayman, P.C., Thebaud, N., Pawley, M.J., et al., Evolution of a ~2.7 Ga large igneous province: a volcanological, geochemical and geochronological study of the Agnew greenstone belt, and new regional correlations for the Kalgoorlie terrane (Yilgarn craton, western Australia), *Precambrian Res.,* 2015, vol. 270, pp. 334–368.

Hoek, J.D., Mafic Dykes of the Vestfold Hills, East Antarctica. An Analysis of the Emplacement Mechanism of Tholeiitic Dyke Swarms and of the Role of Dyke Emplacement during Crustal Extension, *PhD thesis,* Utrecht University, 1994.

Hölttä, P., Balagansky, V., and Garde, A., Archean of Greenland and Fennoscandia, *Episodes,* 2008, vol. 31, no. 1, pp. 13–19.

Irvine, T.N. and Baragar, W.R.A., A guide to the chemical classification of the common volcanic rocks, *Can. J. Earth Sci.,* 1971, vol. 8, pp. 523–548.

Johansson, Å., Bingen, B., Huhma, H., et al., A geochronological review of magmatism along the external margin of Columbia and in the Grenville-age orogens forming the core of Rodinia, *Precambrian Res.,* 2022, vol. 371, 106463.

Kalsbeek, F. and Taylor, P.N., Chemical and isotopic homogeneity of a 400 km long basic dyke in central West Greenland, *Contrib. Mineral. Petrol.,* 1986, vol. 93, no. 4, pp. 439–448.

Kingsbury, C.G., Klausen, M.B., Soderlund, U., et al., Identification of a new 485 Ma post-orogenic mafic dyke swarm east of the Pan-African Saldania–Gariep belt of South Africa, *Precambrian Res.,* 2021, vol. 354, p. 106043.

Klausen, M.B., Conditioned duality between supercontinental 'assembly' and 'breakup' lips, *Geosci. Front.,* 2020, vol. 11, no. 5, pp. 1635–1649.

Klein, E.M., Geochemistry of the igneous oceanic crust, *Treatise Geochem.,* 2003, vol. 3, pp. 433–463.

Kozlov, N.E., Sorokhtin, N.O., Glaznev, V.N., et al., *Geologiya arkheya Baltiiskogo shchita* (Archean Geology of the Baltic Shield), St. Petersburg: Nauka, 2006.

Krogh, T.E., A low-contamination method for hydrothermal decomposition of zircon and extraction of U and Pb for isotopic age determinations, *Geochim. Cosmochim. Acta,* 1973, vol. 87, pp. 485–494.

Krogh, T., Corfu, F., Davis, D., Dunning, G.R., et al., Precise U-Pb isotopic ages of diabase dykes and mafic to ultramafic rocks using trace amounts of baddeleyite and zircon, *Mafic Dyke Swarms, Geol. Ass. Canada. Spec. Publ,* 1987, vol. 34, pp. 147–152.

Larionov, A.N., Andreichev, V.A., and Gee, D.G., The Vendian alkaline igneous suite of northern Timan: ion mi-

croprobe U-Pb zircon ages of gabbros and syenite, Geol. Soc. London: *Mem.*, 2004, vol. 30, no. 1, pp. 69–74.

Larionova, Yu.O., Samsonov, A.V., and Shatagin, K.N., Sources of Archean sanukitoids (high-Mg subalkaline granitoids) in the Karelian Craton: Sm-Nd and Rb_Sr isotopic-geochemical evidence, *Petrology,* 2007, vol. 15, no. 6, pp. 530–550.

Li, T., Zhai, M., Peng, P., et al., Ca. 2.5 billion year old coeval ultramafic–mafic and syenitic dykes in eastern Hebei: implications for cratonization of the North China Craton, *Precambrian Res.,* 2010, vol. 180, nos. 3–4, pp. 143–155.

Ludwig, K.R., PbDat for MS-DOS, version 1.21, *U.S. Geol. Survey Open-File Rept.,* 1991, no. 88-542.

Ludwig, K.R., User's manual for Isoplot 3.0, A geochronological toolkit for Microsoft Excel, *Berkley Geochronol. Center, Spec. Publ.,* 2003, no. 4.

Ludwig, K.R., *SQUID 2 rev. 2.50 a User's Manual*, *Berkeley Geochronol. Center Spec. Publ.,* 2009, vol. 5.

Ludwig, K.R., User's manual for ISOPLOT/Ex 3.75. A geochronological toolkit for Microsoft Excel, *Berkeley Geochronology Center Spec. Publ.,* 2012, no. 5.

Macdonald, R., Wilson, L., Thorpe, R.S., and Martin, A., Emplacement of the cleveland dyke: evidence from geochemistry, mineralogy, and physical modelling, *J. Petrol.,* 1988, vol. 29, no. 3, pp. 559–583.

McDonough, W.F. and Sun, S.-S., The composition of the earth, *Chem. Geol.,* 1995, vol. 2541, no. 94, pp. 223–253

Morimoto, N., Fabries, J., Ferguson, A.K., et al., Nomenclature of pyroxenes, *Am. Mineral.,* 1988, vol. 77, pp. 1123–1133.

Oberthür, T., Davis, D.W., and Blenkinsop, T.G., Precise U-Pb mineral ages, Rb-Sr and Sm-Nd systematics for the Great Dyke, Zimbabwe - constraints on Late Archean events in the Zimbabwe Craton and Limpopo Belt, *Precambrian Res.,* 2002, vol. 113, pp. 293–305.

Pearce, J.A., Ernst, R.E., Peate, D.W., and Rogers, C., LIP printing: use of immobile element proxies to characterize large igneous provinces in the geologic record, *Lithos,* 2021, vol. 392–393, 106068.

Pollard, D.D., Elementary fracture mechanics applied to the structural interpretation of dykes, Mafic Dyke Swarms, *Geol. Ass. Canada. Spec. Publ.,* 1987, vol. 34, pp. 5–24.

Pozhilenko, V.I., Serov, P.A., Petrov, V.P., Sm-Nd isotope studies of the Early Precambrian rocks of the Kola region: a brief overview and new data, *Vestn. Kol'sk. NTs RAN,* 2018, vol. 1 (10), pp. 37–49.

Presnall, D.C., Dixon, S.A., Dixon, J.R., et al., Liquidus phase relations on the join diopside—forsterite–anorthite from 1 atm. to 20 kbar: their bearing on the generation and crystallization of basaltic magma, *Contrib. Mineral. Petrol.,* 1978, vol. 66, pp. Ñ. 203–220.

Rannii dokembrii Baltiiskogo shchita (Early Precambrian of the Baltic Shield), Glebovitskii, V.A, Eds., St. Petersburg: Nauka, 2005. Samsonov, A.V., Stepanova, A.V., Salnikova, E.B., et al., Neoarchean mafic dyke swarms in the murmansk craton: petrology, tectonic setting and paleocontinental significance, *Abstract. Int. Conference "Large Igneous Provinces through Earth History: Mantle Plumes, Supercontinents, Climate Change, Metallogeny and Oil–Gas, Planetary Analogues,"* Tomsk: CSTI Publishing house, pp. 2–5.

Shumlyanskyy, L., Ernst, R.E., Albekov, A., et al., The early Statherian (ca. 1800–1750 Ma) Prutivka–Novogol large igneous province of Sarmatia: geochronology and implication for the Nuna/Columbia supercontinent reconstruction, *Precambrian Res.,* 2021, vol. 358, p. 106185.

Sklyarov, E.V. and Fedorovskii, V.S., Magma mingling: tectonic and geodynamic implications, *Geotectonics,* 2006, vol. 40, no. 2, pp. 120–134.

Slabunov, A.I., Stepanova, A.V., Bibikova, E.V., et al., Neoarchean gabbroids of the Fennoscandian Shield Belomorsk Province: geology, composition, and geochronology, *Dokl. Earth Sci.,* 2008, vol. 423, no. 8, pp. 1207–1211.

Söderlund, U. and Johansson, L., A simple way to extract baddeleyite (ZrO_2), *Geochem. Geophys. Geosys.,* 2002, vol. 3, no. 2, pp. 1–7.

Song, S.G., Wang, M.J., Wang, C., and Niu, Y.L., Magmatism during continental collision, subduction, exhumation and mountain collapse in collisional orogenic belts and continental net growth: a perspective, *Sci. China Earth Sci.,* 2015, vol. 58, no. 8, pp. 1284–1304.

Stacey, J.S. and Kramers, J.D., Approximation of terrestrial lead isotope evolution by a two-stage model, *Earth Planet. Sci. Lett.,* 1975, vol. 26, no. 2, pp. 207–221.

Stark, J.C., Wilde, S.A., Soderlund, U., et al., First evidence of Archean mafic dykes at 2.62 Ga in the Yilgarn craton, western Australia: links to cratonisation and the Zimbabwe Craton, *Precambrian Res.,* 2018, vol. 317, pp. 1–13.

Steiger, R.H. and Jäger, E., Subcommission on geochronology: convention on the use of decay constants in geo- and cosmochronology, *Earth Planet. Sci. Lett.,* 1977, vol. 36, no. 3, pp. 359–362.

Stepanova, A.V., Samsonov, A.V., Salnikova, E.B., et al., Paleoproterozoic mafic dyke swarms in archean kola-murmansk and karelia provinces, eastern Fennoscandia: barcode comparison and implications for paleocontinental reconstructions, *The 33rd Nordic Geol. Winter Meeting. Lyngby, Denmark,* 2018. P. 56.

Sun, S.-S. and McDonough, W.F., Chemical and isotopic systematics of oceanic basalts: implications for mantle composition and processes, *Geol. Soc. London: Spec. Publ.,* 1989, vol. 42, pp. 313–345.

Sun, Q., Zhao, X., Xue, C., Seltmann, R., et al., Neoproterozoic tectonic shift from collisional orogenesis to intraplate extension in the Yili block, southern central Asian orogenic belt, *Precambrian Res.,* 2022, vol. 374, p. 106626.

Svetov, S.A., Stepanova, A.V., Chazhengina, S.Yu., et al., Precision (ICP-MS, LA-ICP-MS) analysis of rock and mineral composition: method and assessment of measurement accuracy as exemplified by the Early Precambrian mafic complexes, *Tr. Karel'sk. NTs RAN,* 2015, no. 7, pp. 173–192.

Tait, J., Straathof, G., Soderlund, U., et al., The Ahmeyim great dyke of Mauritania: a newly dated Archaean intrusion, *Lithos,* 2013, vol. 174, pp. 323–332.

Thirlwall, M.F., Long-term reproducibility of multicollector Sr and Nd isotope ratio analysis, *Chem. Geol.,* 1991, vol. 94, no. 2, pp. 85–104.

Timmerman, M.J. and Daly, S., Sm-Nd evidence for Late Archaean crust formation in the Lapland–Kola mobile belt, Kola Peninsula, Russia and Norway, *Precambrian Res.,* 1995, vol. 72, pp. 97–107.

Veselovskiy, R.V., Samsonov, A.V., Stepanova, A.V., et al., 1.86 Ga key paleomagnetic pole from the Murmansk craton intrusions - eastern Murman sill province, NE Fennoscan-

dia: multidisciplinary approach and paleotectonic applications, *Precambrian Res.,* 2019, vol. 324, pp. 126–145.

Villa, I.M., De Bièvre, P., Holden, N.E., and Renne, P.R., IUPAC-IUGS recommendation on the half life of ^{87}Rb, *Geochim. Cosmochim. Acta,* 2015, vol. 164, pp. 382–385.

Vrevskii, A.B., Specifics of the Neoarchean plume–lithospheric processes in the Kola–Norwegian Province of the Fennoscandian Shield: II. Petrology and geodynamic nature of komatiite–tholeiite association, *Petrology,* 2018, vol. 26, no. 3, pp. 246–254.

Wang, H. and Currie, C.A., Magmatic expressions of continental lithosphere removal, *J. Geophys. Res. Solid Earth,* 2015, vol. 120, pp. 7239–7260.

Wang, Q., Zhao, J., Zhang, C., et al., Paleozoic post-collisional magmatism and high-temperature granulite-facies metamorphism coupling with lithospheric delamination of the East Kunlun orogenic belt, NW China, *Geosci. Front.,* 2022, vol. 13, no. 1, p. 101271

Warr, L.N., IMA-CNMNC approved mineral symbols, *Mineral. Mag.,* 2021, vol. 85, no. 3, pp. 291–320.

Wiedenbeck, M., Allé, P., Corfu, F., et al., Three natural zircon standards for U-Th-Pb, Lu-Hf, trace element and REE analyses, *Geostand. Newsl.,* 1995, vol. 19, no. 1, pp. 1–23.

Wilcox, R.E., The idea of magma mixing: history of a struggle for acceptance, *J. Geol.,* 1999, vol. 107, pp. 421–432.

Wilson, A.H., The geology of the Great Dyke, Zimbabwe: crystallization, layering, and cumulate formation in the *Pl* pyroxenite of cyclic unit 1 of the Darwendale subchamber, *J. Petrol.,* 1992, vol. 33, no. 3, pp. 611–663.

Xu, W., Zhao, Z., and Dai, L., Post-collisional mafic magmatism: record of lithospheric mantle evolution in continental orogenic belt, *Sci. China Earth Sci.,* 2020, vol. 63, no. 12, pp. 2029–2041.

Translated by M. Bogina